ACS APPLIED MATERIALS & INTERFACES

Research Article

www.acsami.org

PbS Quantum-Dot Depleted Heterojunction Solar Cells Employing CdS Nanorod Arrays as the Electron Acceptor with Enhanced Efficiency

Xudong Yao,[†] Shangjing Liu,[†] Yajing Chang,[†] Guopeng Li,[†] Longfei Mi,[†] Xiaoming Wang,*[,‡] and Yang Jiang*[,†]

[†]School of Materials Science and Engineering, Hefei University of Technology, Hefei, Anhui 230009, P. R. China

[‡]School of Engineering Technology, Purdue University, West Lafayette, Indiana 47907, United States

Supporting Information

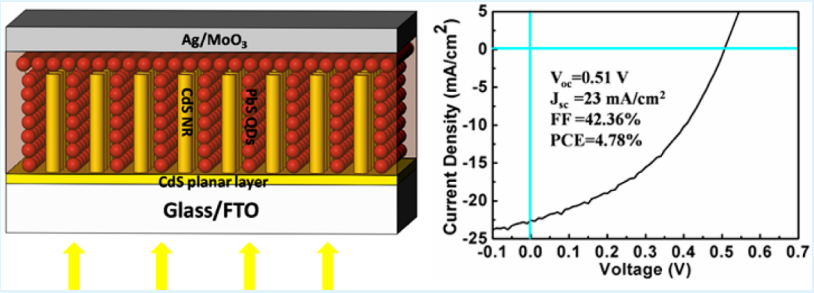

ABSTRACT: Depleted heterojunction (DH) solar cells have shown great potential in power conversion. A 3-D DH structure was first designed and fabricated through a layer-by-layer spin-coating technique to increase the interfacial contact of p-type PbS quantum dots (QDs) and n-type CdS nanorod arrays. As a result, a decent power conversion efficiency of 4.78% in this structure was achieved, which is five times the efficiency of a planar heterojunction structure of a similar thickness. In the 3-D DH structure, n-type CdS nanorod arrays (NRs) were grown vertically as electron acceptors, on which p-type PbS quantum dots were deposited as absorbing materials in a layer-by-layer spin-coating fashion. The results are discussed in view of effective transportation of electrons through CdS NRs than the hopping transportation in large nanoparticle-based CdS film, the enlarged interfacial area, and shortened carrier diffusion distance.

KEYWORDS: *CdS nanorod arrays, PbS quantum dots, solar cells, depleted heterojunction, power conversion efficiency*

1. INTRODUCTION

The next-generation solar cells (such as dye-sensitized solar cells,[1] quantum dot solar cells) are increasingly required to offer the simultaneous combination of low cost and desired high efficiency. In this area, great attention has been paid to PbS QDs for photovoltaic applications mainly due to its quantum-size-effect-tuning to cover the optimal band gap range for solar cells.[2] In addition, PbS QDs can be produced by a simple solution process, and PbS QDs are stable under ambient working conditions. The power conversion efficiency of PbS QDs solar cells has been increased to more than 8% from less than 1% a decade ago attributed to a rational manipulation of the electronic properties of PbS QDs and improved device architecture.[3] An appropriate ligand exchange process plays a significant role in the technology advances by passivating the surface of PbS QDs.[4−6]

While great effort has been made on the surface chemistry of PbS QDs, novel device structures and materials also contributed to the improved photovoltaic performance.[7−10] From Schottky to DH structure, photovoltaic performance has been greatly improved.[11] A typical design relies on wide-bandgap n-type heteropartners, such as TiO_2 and ZnO, to form a rectifying junction with p-type PbS QDs film. In this structure, most of the sunlight will be absorbed by the PbS QDs layer, creating high-density charge carriers near or in the built-in electric field, benefiting both charge separation and transfer. Despite these advantages of the DH structure, the photovoltaic performance is still limited by a compromise between light absorption and carrier extraction.[12] Therefore, novel photoelectrodes were investigated. For example, TiO_2 mesoporous nanoparticle film was introduced to improve collection efficiency by shortening the average minority carrier diffusion length.[13] Also, the interface between light-absorbing materials and electron accepted materials was enlarged greatly, contributing to the enhanced overall energy conversion efficiency. However, a recombination loss occurred in the collection of the photogenerated electrons because of the random network of nanocrystalline TiO_2. In contrast to the

Received: July 27, 2015
Accepted: September 29, 2015
Published: September 29, 2015

© 2015 American Chemical Society

DOI: 10.1021/acsami.5b06857
ACS Appl. Mater. Interfaces 2015, 7, 23117−23123

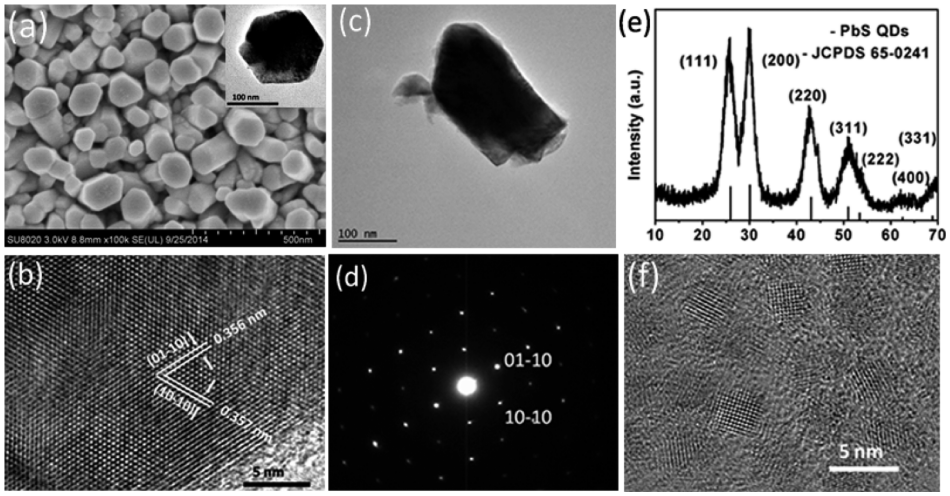

Figure 1. (a) FESEM image of the top-surface of pure CdS NRs with the top-view of an individual CdS NR shown in the inset. (b) HRTEM image of a single-crystalline CdS NR. (c) TEM image of an individual CdS nanorod. (d) Electron diffraction pattern of CdS with a zone axis ⟨0001⟩. (e) XRD patterns. (f) HRTEM image of resulting PbS QDs.

disordered nanoporous matrix structure, one-dimensional ordered nanostructures offer direct and efficient pathways for photogenerated electrons, reduce interparticulate boundaries, and avoid a series of particle-to-particle hopping transport.[14] In the past few years, ZnO[15] and TiO_2[16] nanowires and NRs were interpenetrated with PbS QDs to improve charge separation and collection, which led to a higher photocurrent than that of a planar structure. However, a conduction-band offset threshold and limited candidate materials undoubtedly still limit the application of PbS QDs in different sizes.[17] So it is necessary to develop new n-type electrode materials.[18−20] CdS, which is widely used as an electron acceptor layer in the field of CdS/CdTe solar cells, has therefore been considered as an alternative heteropartner with PbS QDs.[21−23] Bawendi et al. first chose chemical-bath-deposited (CBD) CdS to form a heterojunction with PbS QDs and obtained an average 3.5% energy efficiency.[24] Also, Yang et al. prepared oriented and high-density CdS NR arrays embedded in PbS thin films,[18] In their work, both the n-type CdS and p-type PbS thin film were prepared by the CBD method, and these novel device structures with larger surface area and improved carrier diffusion distance are potentially useful for advanced solar cells. Finally, an efficiency of 1.01% had been achieved in their report. However, compared to the solution-processed QDs, the bandgap of PbS NC prepared by the CBD method did not easily cover the optimal band gap range for DH solar cells, which may restrict the application in the DH device.

In this study, we first constructed a 3-D DH PbS QDs solar cells employing CdS NRs as electron acceptor. The PbS QDs were synthesized through the solution process method, and the CdS NRs were synthesized through a facile two-step template-free hydrothermal approach, which allows PbS QDs to infiltrate into the CdS nanorod arrays by spin-coating to form a new 3-D DH structure. By optimizing the processing conditions, we successfully infiltrated PbS QDs into NRs completely to obtain an interpenetrating network of NRs and QDs with larger heterojunction area and shortened carrier diffusion distance effectively. The highest power conversion efficiency of 4.78% has been achieved, approximately five times higher than that of a planar design of similar thickness. Also, the efficiency presented here was higher than that of previously reported CdS NRs/PbS QDs based solar cells.

2. EXPERIMENTAL DETAILS

Detailed description about the synthesis of PbS QDs has been given in one of our previous papers.[25] With the increase of injection temperature and the concentration of OA, the size of QDs becomes larger. In order to obtain a suitable size of QDs for assembling the solar cells, we control the injection temperature at 120 °C and OA concentration in 0.2 mol/kg. Typically, 0.45 g of PbO, 1.5 mL of oleic acid, and 18 mL of ODE were mixed in a three-neck round-bottom flask in a typical synthesis. The flask was heated to 120 °C, then 200 μL TMS in 10 mL ODE solution was injected into the above solution, which changed to a brownish color immediately, as evidence of the formation of PbS QDs.[26,27] Finally, the product was dispersed in toluene for storage.

2.1. Materials. All the chemicals were used as received. PbO (>99%), cadmium chloride [$CdCl_2·2.5H_2O$ >99%], thiourea [$CS(NH_2)_2$ >99%], NH_4Cl (>99.5%), KOH (>85%), cadmium nitrate [$Cd(NO_3)_2·4H_2O$ >99%], and NH_4OH (25−28%) were purchased from Sinopharm Chemical Reagents Co. Ltd.; oleic acid (OA, tech. grade, 90%), 1-octadecene (ODE, tech. grade, 90%), and 3-mercaptopropionic acid (MPA 98%) were purchased from Aladdin; bis(trimethylsilyl) sulfide (TMS, 97%) was purchased from Sigma-Aldrich.

2.2. Device Fabrication. FTO substrates were cleaned thoroughly in emulsifier, acetone, ethanol, and deionized water for 30 min sequentially in an ultrasonic bath and were dried in a nitrogen atmosphere. Then arrays of CdS nanorods were produced on the well-cleaned FTO substrate via a two-step process. First, a seed layer of CdS crystals was deposited on the FTO as a protective layer by CBD method in 350 mL aqueous solution containing cadmium chloride [$CdCl_2·2.5H_2O$] (0.40 g), thiourea [$CS(NH_2)_2$] (1.33 g), NH_4Cl (10.52 g), and KOH (2.45 g). During the deposition, the temperature was maintained at 80 °C and the duration varied from 5 to 15 min. After the deposition, the film was cleaned by deionized water to remove residual precursors and loosely bound CdS nanoparticles. Then NRs were grown by transferring the CdS-coated FTO glass into a Teflon-lined stainless autoclave. The solution that was used for the preparation of CdS nanorod arrays consists of 0.5 mmol cadmium nitrate [$Cd(NO_3)_2·4H_2O$], 1.5 mmol thiourea, and 40 mL deionized water. The temperature was heated to 200 °C and maintained for 12 h. For this 3D DH structure, the NRs with a suitable length of ∼300 nm were obtained. Planar CdS NC thin film was used as in a previously reported method.[25] A deposition time of 30 min was used to produce CdS film with a similar thickness comparable to the height of the NRs. The substrates were rinsed with deionized water and dried by nitrogen.

A PbS QDs nanoink was spin-coated at 4000 rpm onto the substrate to infiltrate the interspaces of CdS nanorod arrays to

DOI: 10.1021/acsami.5b06857
ACS Appl. Mater. Interfaces 2015, 7, 23117−23123

construct a 3-D DH structure similar to the method reported earlier.[25] Before spin-coating PbS films, the PbS QDs were washed with methane/toluene of 1:1 twice, and then redispersed in octane to produce 50 mg/mL nanoink; the details of PbS QDs deposition process were as follows: (1) 2 drops of ink were deposited on the substrate; (2) 400 μL 1% MPA/methane solution; (3) 10 drops of methane solution; (4) 10 drops of methane solution. The above operations were repeated 6 times. All spin-coating steps were at 4000 rpm. The spin time was set at 15 s. Finally, 10 nm of MoO_3 was deposited by thermal evaporation under a pressure of $(1-5) \times 10^{-5}$ Torr with a rate of 0.03–0.04 nm/s while Ag electrode was deposited on MoO_3 layer at a rate of 0.02–0.03 nm/s to a thickness of 150 nm. An active area was 0.09 cm^2.

2.3. Device Characterization. The morphology of the sample was analyzed by a field-emission scanning electron microscope (FESEM) (SU8020). High-resolution images were taken by using a high-resolution transmission electron microscope (TEM) (JEM-2100). The absorption spectra of PbS QDs in toluene and the transmission spectra of CdS films and CdS/PbS films were measured using Shimadzu UV–vis-NIR 3600 spectrophotometer. Photocurrent density–voltage (J–V) measurements were conducted using a Keithley 2636 system sourcemeter and a Xenon Lamp Solar Simulator equipped with an AM 1.5 filters under N_2 atmosphere. The monochromatic incident photon-to-electron conversion efficiency (IPCE) was tested using Zolix spectrograph, where illumination was provided by a xenon lamp, with standard silicon cell (OPRC185Si.QG-CAL S/N #1138) as reference.

3. RESULTS AND DISCUSSION

A typical top-surface of the as-prepared CdS nanorod arrays that were prepared by this two-step solution approach is shown in Figure 1a, an FESEM image. It is obvious that the entire surface of the FTO substrate is covered uniformly with CdS NRs, which could lead to an increased surface area compared to a planar surface. The cross section size of the NRs varies from 60 to 150 nm in a hexagonal shape, a character of hexagonal CdS crystal growing along its ⟨0001⟩ direction. The nanorod arrays with space among them are suitable for the fabrication of solar cells with a 3-D structure using a spin-coating method. The top-view of an individual CdS NR is shown in the inset and its corresponding HRTEM image is shown in Figure 1b. The fringe spaces of 0.356 and 0.357 nm in the HRTEM image are consistent with the crystal constants of (01–10) and (10–10) planes of hexagonal wurtzite CdS. Figure 1c displays the TEM image of a single CdS NR. The length of the CdS NR is approximately 300 nm, and the diameter is about 137 nm. In addition, an electron diffraction pattern of a CdS NR, as shown in Figure 1d, reveals that the NR is single crystalline in nature and grows along its [0001] direction preferentially. The XRD pattern of PbS QDs presents a rock salt structure in the Figure 1e. All of the diffraction peaks can be indexed to PbS (JCPDS# 65–0241). A high-resolution TEM image of PbS QDs is presented in Figure 1f. The well-resolved and continuous fringes indicate that the PbS QDs is single crystalline and the mean size is ~3.5 nm.

In order to show the formation of an interpenetrating 3-D DH structure, the top-surface of CdS NRs substrate during the spin-coating process was monitored. Figure 2a–d presents the top-surfaces of CdS NRs that are coated with PbS QDs after different spin-coating cycles. In Figure 2a, after the deposition of the first layer, the nanorod morphology was well preserved, which demonstrates the filling of the porous structure. With further increase in the deposition cycles, the void space between the nanorod arrays is slowly filled up by PbS QDs. As shown in Figure 2c, when the spin coating cycle reached 4, no

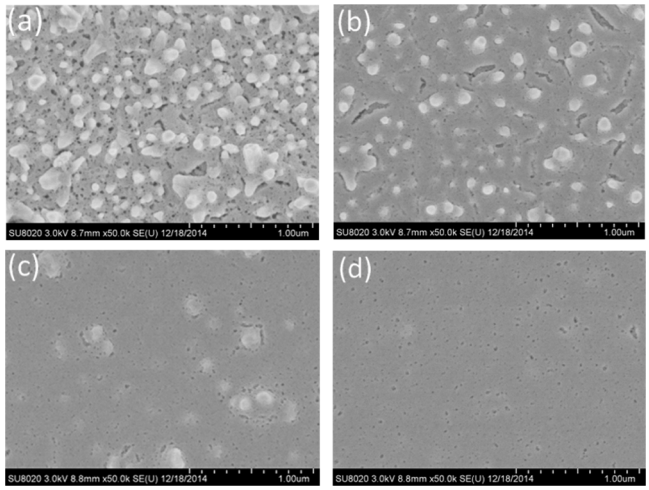

Figure 2. FESEM images of the top-surface of CdS NR/PbS QDs heterojunction based on different deposition cycles: (a) 1 cycle, (b) 2 cycles, (c) 4 cycles, and (d) 6 cycles.

NRs can be seen obviously, evidence of the formation of an interpenetrating network structure of PbS QDs and CdS nanorod arrays. Two more layers of PbS QDs were coated to obtain a compact and flat PbS film. The infiltration rate of PbS QDs, which determines the performance of the final device, depends sensitively on spin-coating processing parameters, including the speed of spin-coating, the shape or size of the substrate, and the concentration of PbS QDs solution.

To further study whether the gap in the CdS NR arrays is filled completely by PbS QDs, the morphology of a 6-layer PbS QDs coated NR device was further analyzed. The corresponding cross-sectional SEM image of the device was shown in Figure 3b. The active layer of the device with a thickness ~500 nm, as sandwiched between FTO and top electrode, is presented well in the image. More importantly, typical nanorod features are visibly shown and no void space can be observed, suggesting the successful construction of 3-D DH structure. Also, we carried out EDS mapping of the elemental distribution in the cross-section to demonstrate that p-type PbS quantum

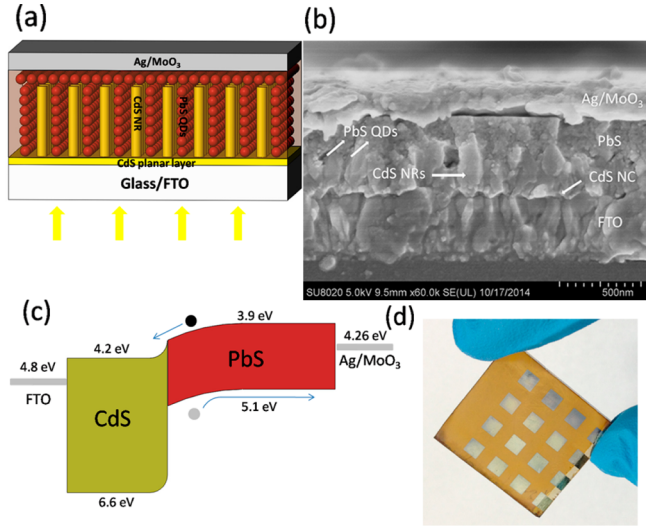

Figure 3. (a) Structure of device. (b) Cross-sectional FESEM image of CdS NRs/PbS QDs heterojunction. (c) Energy band diagram and photocarrier transport mechanism. (d) Photograph of a solar cell.

DOI: 10.1021/acsami.5b06857
ACS Appl. Mater. Interfaces 2015, 7, 23117–23123

dots are filled in the gaps between n-type CdS nanorod arrays shown in the Figure S-4. The position of Pb is consistent with the position of Cd, indicating that the void space between the nanorod arrays is really filled up by PbS QDs. The 3-D heterojunction structure is presented in Figure 3a. Illumination is made from the CdS side. The high density photocarriers are mainly produced in the large interfacial area between photoactive materials and electron accepted materials. Then photogenerated electrons pass along the NRs to the FTO side. The energy levels of the constituent materials taken from the literature are shown in Figure 3c.[24,28] In the CdS/PbS QDs interface, a space charge region and a built-in electric field (with a direction from CdS to PbS) are formed due to the diffusion of the majority carriers. The built-in electric field causes a drift of majority carriers. Finally a balance between drift current and diffusion current is achieved in the p−n junction. Under illumination, the photogenerated minority carriers (electrons) within the combined diffusion length and in the depletion width region sweep into the CdS layer, while the holes move in an opposite direction and the photocurrent with the direction from n-type CdS to p-type PbS QDs. As indicated in the energy level diagram, the Fermi level of p-type PbS QDs is higher than the work function of Ag (−4.26 eV), therefore inducing an electron transfer from the metallic electrode to PbS QDs, forming the Schottky junction in the PbS QDs/Ag interface. The built-in electric field in the Schottky junction has the direction from the metal to the PbS QDs, which would inhibit hole transport to the metal electrode, while the insertion of MoO_3 is proven to remove a downward band-bending, pin the Fermi level of the top electrode, and inhibit the formation of the Schottky junction, which improves the performance of the cells dramatically.[29]

Because the performance of the device is highly dependent on the fill rate of absorbing layer in the 3-D heterojunction solar cells, the transmission spectrum of different PbS QDs deposition cycles were studied to maximize the device performance. The PbS QDs with the first excitonic absorption peak at 1071 nm (see Supporting Information, Figure S-1) are introduced to assemble the device for the transmission spectrum of various PbS QDs layers. In order to eliminate the effect of FTO absorption and only measure the transmittance of CdS and CdS/PbS QDs film, we used blank FTO substrate as the base and assumed that its transmittance is 100%. As shown in Figure 4a, a sharp increase of transmission occurs from 500 to 520 nm. The absorption near 520 nm is regarded as the intrinsic band gap absorption of CdS (2.4 eV) attributed to the electron transitions from the valence band to the conduction band. The absorption of CdS in the wavelength range above 600 nm is generally attributed to a light-scattering effect. With further increase in the number of PbS layers, the characteristic absorption of CdS becomes unclear while the PbS QDs absorption trend becomes obvious (the light absorbance extends to the region from visible to near-infrared). After 6 cycles of deposition, the curve fits to the PbS absorption spectrum, indicating that the overlay region is formed above the CdS nanorod arrays, in accordance with the cross-sectional image in Figure 3b. Furthermore, the position of the valley in the transmission matches perfectly with that of the first excitonic absorption peak, proving a high stability of quantum dots in the assembly of the device. Representative $J-V$ curves for this 3-D structure with various layers (1, 2, 4, 6) are presented in Figure 4b, and the photovoltaic parameters are summarized in Table 1. The increase of J_{sc} from 2.35 mA/cm^2

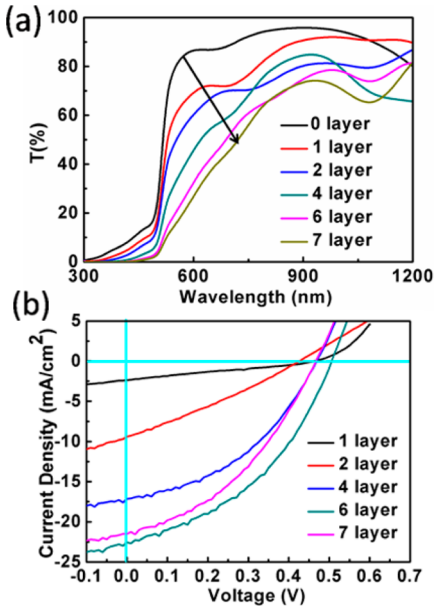

Figure 4. (a) Transmittance spectrum of thin films with different PbS layers. (b) Representative $J-V$ characteristics of the 3D heterojunction solar cells based on different PbS layers.

Table 1. Performance of the 3D Structure Devices with Different Spin-Coating Cycles

cycles	J_{sc} (mA/cm^2)	V_{oc} (V)	FF (%)	PCE (%)
1	2.35	0.47	29.14	0.31
2	9.28	0.43	30.81	1.33
4	17.59	0.47	43.64	3.44
6	23.00	0.51	42.36	4.78
7	21.49	0.47	40.87	4.00

to 23.0 mA/cm^2 with the increasing cycles of spin-coating process is observed. It is attributed to the effective infiltration of PbS QDs into CdS nanorod arrays and the formation of good quality 3-D DH. For a thinner PbS layer, the V_{oc} is high, indicating that the photocarriers can be extracted easily in the depletion region. In Figure 2 a,b, PbS QDs do not completely cover the CdS NRs arrays, causing some direct contact between CdS NRs and metal electrode; this may affect the electronic characteristic of device by short circuit in heterojunction application, which is considered to be the main reason for poor FF as shown in Figure 4b. Since the PbS QDs absorbing layer is too thin, the J_{sc} is very low. When the cycle increased to 6, flat and continuous PbS QDs films have been formed, the PCE of the NRs device increases to 4.78%, and the V_{oc}, J_{sc}, and FF are 0.51 V, 23.0 mA/cm^2, and 42.36%, respectively. Further increase in the number of cycles results in a small decrease in the J_{sc}, V_{oc}, FF, and PCE of devices. From the cross-section of Figure 3b, PbS QDs fully cover the NRs when the number of cycles is increased to 6. Therefore, thicker overlay caused by more deposition cycles on top of the NRs may result in more absorption of light, while the built-in potential in the depletion region is not sufficient to assist photocarriers in the process of collecting to the metal electrode without recombination.

For comparison, a CdS planar electrode device with a similar thickness to the nanorod arrays was deposited. After 6 cycles of deposition, a compact and relatively flat PbS QDs film was obtained as shown in the Supporting Information (Figure S-2b). It can be seen from the FESEM image in Figures S-2a that

DOI: 10.1021/acsami.5b06857
ACS Appl. Mater. Interfaces 2015, 7, 23117−23123

the CdS film surface appears to be uniform throughout without pinholes, which may affect the electronic characteristics of the device by short circuit in heterojunction application. Clearly, the thickness of the CdS planar layer is about 300 nm and the PbS thickness is about 350 nm (see the Supporting Information Figure S-2c). Figure 5a shows the $J-V$ characteristics of the

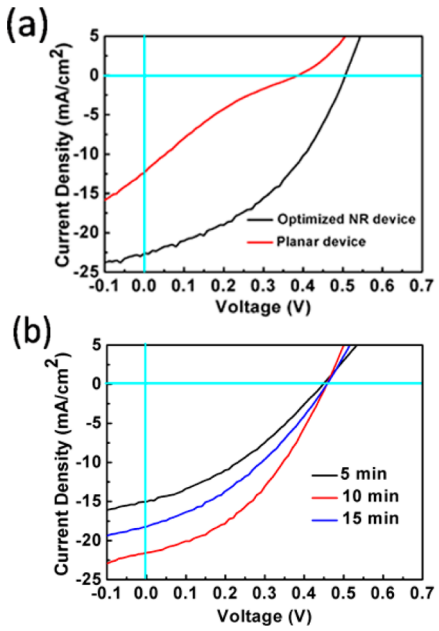

Figure 5. (a) $J-V$ characteristics of the best 3D heterojunction device and the representative planar device with similar CdS thickness. (b) The representative $J-V$ characteristics of the NR solar cells based on various thicknesses of CdS planar layer.

best NR device and a typical planar device. As pointed out in our previous work,[25] the increase in thickness of the CdS layer resulted in a rapid decrease of PCE in the solar cells. When the CBD time increased to 30 min, we obtained a dense CdS layer with the thickness of about 300 nm, a similar thickness with NR. Also, the PCE decreases to 0.91% and the J_{sc}, V_{oc}, and FF are 12.62 mA/cm^2, 0.39 V, and19.37%, respectively. For the NR device, the highest PCE of 4.78% is obtained. The J_{sc} and V_{oc} were measured as 23.0 mA/cm^2 and 0.51 V, respectively, with a FF 42.36%. The great performance advance in the NR device compared to that of a planar one can be attributed to the following reasons. First, the interfacial area between light-active materials and electron acceptor materials is greatly enlarged, which improves charge separation.[30] Second, compared to large nanoparticle-based CdS film, the ordered NRs offer direct electrical pathways for photogenerated electrons by avoiding the particle-to-particle hopping, which induces the recombination in the collection of photogenerated electrons. Third, the larger surface roughness of PbS QDs film that is caused by thicker CdS planar film produces traps easily. The traps capture holes and impede the transport of holes, resulting in unbalanced electron and hole pairs. This increases the reverse saturation current density and leads to the decline of FF and V_{oc} as reported.[25] Finally, the increased thickness in the planar structure causes high series resistance, directly leading to a poor FF, which deteriorates the performance of the cells.

Additionally, the IPCE spectrum in Figure 6 reveals that the high current is a direct result of the increased total absorption in a broad wavelength range from ultraviolet to near-infrared.

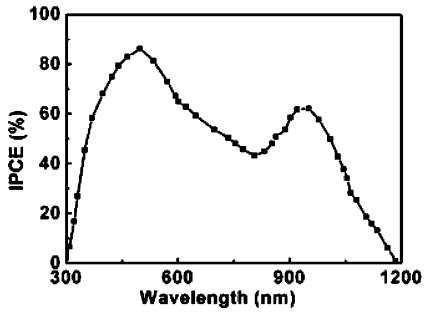

Figure 6. IPCE spectra for the best device.

The IPCE increases rapidly and reaches the maximum at a wavelength of 500 nm, which closely matches the bandgap of CdS (2.4 eV). The IPCE peak at 940 nm is consistent with the first excitation absorption peak of PbS QDs in octane. The device stability was tested over a period of 6 days. The evolution of device performance parameters with air storage time was shown in Figure 7. The devices were tested under

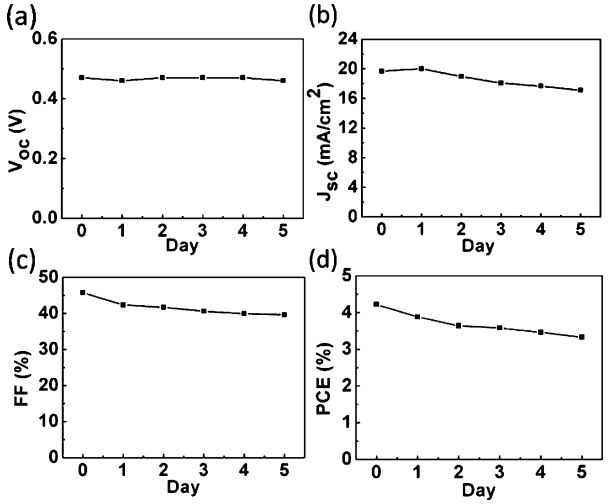

Figure 7. Stability testing of the device. (a) Open circuit voltage (V_{oc}). (b) Short-circuit current (J_{sc}). (c) Fill factor (FF). (d) Power conversion efficiency (PCE).

nitrogen. The open circuit voltage exhibits good stability. The short circuit current and fill factor exhibit a gradual decline and saturation at less than 13% decreased performance. The PCE declines at less than 24% decrease after 6 days. In a word, this slight decline in performance with time also holds promise for the next encapsulation strategies to maintain performance.

The deposition time of a seed CdS layer is crucial in producing high-performance devices. As shown in the $J-V$ curve (Figure 5b), better performance can be achieved after a deposition time of 10 min. When the deposition time is increased to 15 min, the J_{sc} begins to decrease. To investigate the mechanism of this time-dependent performance, the top-surface morphology during the deposition process was analyzed by FESEM. For a deposition time of 30 min (see the Supporting Information Figure S-5), the space between the NRs has almost totally disappeared and the top-surface has become dense but uneven with hexagonal nanoparticles, making it hard for PbS QDs to infiltrate into the nanorod arrays.

DOI: 10.1021/acsami.5b06857
ACS Appl. Mater. Interfaces 2015, 7, 23117−23123

4. CONCLUSION

3-D DH solar cells were fabricated successfully by using vertically aligned CdS nanorod arrays and solution-processed PbS colloidal quantum dots. A 3-D dense heterojunction structure was obtained and a decent power conversion efficiency of 4. 78% was achieved, resulting in up to a 5-fold increase compared to the CdS planar layer owning the similar thickness with the NRs. There are still a lot of possibilities in improving the PV efficiency, including annealing the NRs to increase crystallinity, adjusting the interval and length of the NRs, and improving the contact between CdS NRs and PbS QDs. These are worthy of further exploration.

■ ASSOCIATED CONTENT

Supporting Information

The Supporting Information is available free of charge on the ACS Publications website at DOI: 10.1021/acsami.5b06857.

Figure S-1. Absorption spectra of the PbS QDs in toluene. Figure S-2. FESEM images of the top-surface of the CdS film (a) and PbS film (b), and the cross-sectional FESEM image of the planar heterojunction structure (c). Figure S-3. XPS spectrum of CdS NRs and PbS QDs: (a) Cd 3d spectrum, (b) S 2p spectrum of CdS NRs, (c) Pb 4f spectrum, (d) S 2p spectrum of PbS QDs. Figure S-4. EDS mapping of the elemental distribution in the cross-section of the device. Figure S-5. FESEM image of the top-surface of the CdS NR film with the deposition time of 30 min (PDF)

■ AUTHOR INFORMATION

Corresponding Authors

*E-mail: apjiang@hfut.edu.cn. Fax/Tel: +86-551-62904358.
*E-mail: wang1747@purdue.edu. Tel: 765-4966092. Fax:765-4946219.

Notes

The authors declare no competing financial interest.

■ ACKNOWLEDGMENTS

We thank the National High Technology Research and Development Program of China (No. 2007AA03Z301, 2013AA03A114), the National Natural Science Foundations of China (No.61076040), and the Specialized Research Fund for the Doctoral Program of Higher Education of China (No. 2012011111006) for financial support.

■ REFERENCES

(1) Liu, Z.; Han, J.; Guo, K.; Zhang, X.; Hong, T. Jalpaite Ag_3CuS_2: A Novel Promising Ternary Sulfide Absorber Material For Solar Cells. *Chem. Commun.* **2015**, *51*, 2597−2600.

(2) Lee, H. J.; et al. Regenerative PbS and CdS Quantum Dot Sensitized Solar Cells with a Cobalt Complex as Hole Mediator. *Langmuir* **2009**, *25*, 7602−7608.

(3) Chuang, C.-H. M.; Brown, P. R.; Bulović, V.; Bawendi, M. G. Improved Performance and Stability in Quantum Dot Solar Cells through Band Alignment Engineering. *Nat. Mater.* **2014**, *13*, 796−801.

(4) Tang, J.; Brzozowski, L.; Barkhouse, D. A. R.; Wang, X.; Debnath, R.; Wolowiec, R.; Palmiano, E.; Levina, L.; Pattantyus-Abraham, A. G.; Jamakosmanovic, D.; et al. Quantum Dot Photovoltaics in the Extreme Quantum Confinement Regime: the Surface-chemical Origins of Exceptional Air-and Light-stability. *ACS Nano* **2010**, *4*, 869−878.

(5) Crisp, R. W.; Kroupa, D. M.; Marshall, A. R.; Miller, E. M.; Zhang, J.; Beard, M. C.; Luther, J. M. Metal Halide Solid-State Surface Treatment for High Efficiency PbS and PbSe QD Solar Cells. *Sci. Rep.* **2015**, *5*, 9945.

(6) Park, J. P.; Heo, J. H.; Im, S. H.; Kim, S. W. Exceptional Stability of Mg-implemented PbS Quantum Dot Solar Cells Realized by Galvanic Corrosion Protection. *J. Mater. Chem. A* **2015**, *3*, 8433.

(7) Hjerrild, N. E.; Neo, D. C. J.; Kasdi, A.; Assender, H. E.; Warner, J. H.; Watt, A. A. Transfer Printed Silver Nanowire Transparent Conductors for PbS-ZnO Heterojunction Quantum Dot Solar Cells. *ACS Appl. Mater. Interfaces* **2015**, *7*, 6417.

(8) Wang, X.; Koleilat, G. I.; Tang, J.; Liu, H.; Kramer, I. J.; Debnath, R.; Brzozowski, L.; Barkhouse, D. A. R.; Levina, L.; Hoogland, S.; et al. Tandem Colloidal Quantum Dot Solar Cells Employing a Graded Recombination Layer. *Nat. Photonics* **2011**, *5*, 480−484.

(9) Saha, S. K.; Bera, A.; Pal, A. J. Improvement in PbS-based Hybrid Bulk-Heterojunction Solar Cells through Band-Alignment via Bismuth Doping in the Nanocrystals. *ACS Appl. Mater. Interfaces* **2015**, *7*, 8886.

(10) Brennan, T. P.; Trejo, O.; Roelofs, K. E.; Xu, J.; Prinz, F. B.; Bent, S. F. Efficiency Enhancement of Solid-state PbS Quantum Dot-sensitized Solar Cells with Al_2O_3 Barrier Layer. *J. Mater. Chem. A* **2013**, *1*, 7566−7571.

(11) Pattantyus-Abraham, A. G.; Kramer, I. J.; Barkhouse, A. R.; Wang, X.; Konstantatos, G.; Debnath, R.; Levina, L.; Raabe, I.; Nazeeruddin, M. K.; Gratzel, M.; et al. Depleted-heterojunction Colloidal Quantum Dot Solar Cells. *ACS Nano* **2010**, *4*, 3374−3380.

(12) Lan, X.; Masala, S.; Sargent, E. H. Charge-extraction Strategies for Colloidal Quantum Dot Photovoltaics. *Nat. Mater.* **2014**, *13*, 233−240.

(13) O'Hayre, R.; Nanu, M.; Schoonman, J.; Goossens, A. A Parametric Study of $TiO_2/CuInS_2$ Nanocomposite Solar Cells: How Cell Thickness, Buffer Layer Thickness, and TiO_2 Particle Size Affect Performance. *Nanotechnology* **2007**, *18*, 055702.

(14) Zhou, Z.-j.; Fan, J.-q.; Wang, X.; Sun, W.-z.; Zhou, W.-h.; Du, Z.-l.; Wu, S.-x. Solution Fabrication and Photoelectrical Properties of CuInS2 Nanocrystals on TiO2 Nanorod Array. *ACS Appl. Mater. Interfaces* **2011**, *3*, 2189−2194.

(15) Liu, C.; Liu, Z.; Li, Y.; Ya, J.; Lei, E.; An, L. CdS/PbS Co-sensitized ZnO Nanorods and its Photovoltaic Properties. *Appl. Surf. Sci.* **2011**, *257*, 7041−7046.

(16) Tao, L.; Xiong, Y.; Liu, H.; Shen, W. High Performance PbS Quantum Dot Sensitized Solar Cells via Electric Field Assisted in situ Chemical Deposition on Modulated TiO_2 Nanotube Arrays. *Nanoscale* **2014**, *6*, 931−938.

(17) Liu, H.; Tang, J.; Kramer, I. J.; Debnath, R.; Koleilat, G. I.; Wang, X.; Fisher, A.; Li, R.; Brzozowski, L.; Levina, L.; et al. Electron Acceptor Materials Engineering in Colloidal Quantum Dot Solar Cells. *Adv. Mater.* **2011**, *23*, 3832−3837.

(18) Sun, M.; Fu, W.; Li, Q.; Yin, G.; Chi, K.; Ma, J.; Yang, L.; Mu, Y.; Chen, Y.; Su, S.; et al. Embedded CdS Nanorod Arrays in PbS Absorber Layers: Enhanced Energy Conversion Efficiency in Bulk Heterojunction Solar Cells. *RSC Adv.* **2014**, *4*, 7178−7184.

(19) Chen, F.; Zhou, R.; Yang, L.; Shi, M.; Wu, G.; Wang, M.; Chen, H. One-step Fabrication of CdS Nanorod Arrays via Solution Chemistry. *J. Phys. Chem. C* **2008**, *112*, 13457−13462.

(20) Nam, M.; Park, J.; Lee, K.; Kim, S. W.; Ko, H.; Han, I. K.; Ko, D. H. A Multifunctional Fullerene Interlayer in Colloidal Quantum Dot-based Hybrid Solar Cells. *J. Mater. Chem. A* **2015**, *3*, 10585.

(21) Bhandari, K. P.; Roland, P. J.; Mahabaduge, H.; Haugen, N. O.; Grice, C. R.; Jeong, S.; Dykstra, T.; Gao, J.; Ellingson, R. J. Thin Film Solar Cells Based on the Heterojunction of Colloidal PbS Quantum Dots with CdS. *Sol. Energy Mater. Sol. Cells* **2013**, *117*, 476−482.

(22) Rakhshani, A. Heterojunction Properties of Electrodeposited CdTe/CdS Solar Cells. *J. Appl. Phys.* **2001**, *90*, 4265−4271.

(23) Fan, Z.; Razavi, H.; Do, J.-w.; Moriwaki, A.; Ergen, O.; Chueh, Y.-L.; Leu, P. W.; Ho, J. C.; Takahashi, T.; Reichertz, L. A.; et al. Three-dimensional Nanopillar-array Photovoltaics on Low-cost and Flexible Substrates. *Nat. Mater.* **2009**, *8*, 648−653.

(24) Chang, L.-Y.; Lunt, R. R.; Brown, P. R.; Bulović, V.; Bawendi, M. G. Low-temperature Solution-processed Solar Cells Based on PbS

DOI: 10.1021/acsami.5b06857
ACS Appl. Mater. Interfaces 2015, 7, 23117−23123

Colloidal Quantum Dot/CdS Heterojunctions. *Nano Lett.* **2013**, *13*, 994−999.
(25) Yao, X.; Chang, Y.; Li, G.; Mi, L.; Liu, S.; Wang, H.; Yu, Y.; Jiang, Y. Inverted Quantum-dot Solar Cells with Depleted Heterojunction Structure Employing CdS as the Electron Acceptor. *Sol. Energy Mater. Sol. Cells* **2015**, *137*, 287−292.
(26) Zhang, J.; Crisp, R.; Gao, J.; Kroupa, D. M.; Beard, M. C.; Luther, J. M. Synthetic Conditions for High-accuracy Size Control of PbS Quantum Dots. *J. Phys. Chem. Lett.* **2015**, *6*, 1830.
(27) Hines, M. A.; Scholes, G. D. Colloidal PbS Nanocrystals with Size-tunable Near-infrared Emission: Observation of Post-synthesis Self-narrowing of the Particle Size Distribution. *Adv. Mater.* **2003**, *15*, 1844−1849.
(28) Hyun, B.-R.; Zhong, Y.-W.; Bartnik, A. C.; Sun, L.; Abruna, H. D.; Wise, F. W.; Goodreau, J. D.; Matthews, J. R.; Leslie, T. M.; Borrelli, N. F. Electron Injection from Colloidal PbS Quantum Dots into Titanium Dioxide Nanoparticles. *ACS Nano* **2008**, *2*, 2206−2212.
(29) Brown, P. R.; Lunt, R. R.; Zhao, N.; Osedach, T. P.; Wanger, D. D.; Chang, L.-Y.; Bawendi, M. G.; Bulovic, V. Improved Current Extraction from ZnO/PbS Quantum Dot Heterojunction Photovoltaics Using a MoO3 Interfacial Layer. *Nano Lett.* **2011**, *11*, 2955−2961.
(30) Lan, X.; Bai, J.; Masala, S.; Thon, S. M.; Ren, Y.; Kramer, I. J.; Hoogland, S.; Simchi, A.; Koleilat, G. I.; Paz-Soldan, D.; et al. Self-Assembled, Nanowire Network Electrodes for Depleted Bulk Heterojunction Solar Cells. *Adv. Mater.* **2013**, *25*, 1769−1773.

DOI: 10.1021/acsami.5b06857
ACS Appl. Mater. Interfaces 2015, 7, 23117−23123